© JAN 2026 | IRE Journals | Volume 9 Issue 7 | ISSN: 2456-8880
DOI: https://doi.org/10.64388/IREV9I7-1713855

Synthesis and Characterization of Thin Film Gas Sensors Using Sri Lankan Natural Graphite: Comparative Analysis of Sensitivity to Ammonia, Acetone, and Ethanol Vapors

I.G.P.N. KARUNASENA[1], CHATHURANGA RATHNAYAKE[2], ROSHAN THOTAGAMUGE[3], S.P.A.U.K. SAMARAKOON[4], P. SAMARASEKARA[5]

[1]*Postgraduate Institute of Science, University of Peradeniya, Peradeniya, Sri Lanka*

[2, 5]*Department of Physics, University of Peradeniya, Peradeniya, Sri Lanka*

[3]*Department of Optometry, University of Sri Jayawardenapura, Nugegoda, Sri Lanka*

[4]*Department of Nano Science Technology, Wayamba University of Sri Lanka, Kuliyapitiya, Sri Lanka*

Abstract- ***Gas sensors were synthesized by using Sri Lankan natural graphite as the primary material. Any kind of pure graphite has never been used to identify ammonia, acetone and ethanol vapors. A thin film was coated on Fluorine-doped Tin Oxide (FTO) glass using the doctor blade method, with the graphite mixture prepared using acetone and distilled water and annealed at 100 ^{0}C for two hours in air. Surface morphology analysis via Scanning Electron Microscopy (SEM) revealed closely packed irregular shaped particles ranging in size from approximately 4 to 70 µm. The estimated value of the porosity was found to be 8.98%. X-ray Diffraction (XRD) analysis explored calculated crystallite sizes of 60.00782, 73.19767, and 59.28573 nm for the 002, 004, and 006 planes, respectively. X-ray diffraction patterns reveal that single phase of pure graphite is crystallized in thin film form, and there is not any preferred orientation of crystallites. Gas sensitivity, recovery time, and response time were evaluated in 1000 ppm of ammonia (NH_3), ethanol, and acetone vapors at room temperature. Among these, acetone vapor exhibited the highest sensitivity at 23.98% for 1000 ppm, compared to 6.37% for NH_3 and 7.16% for ethanol. The response and recovery times for acetone vapor were 50 and 22 minutes, respectively. All the samples were measured for three adsorption and desorption cycles to study the repetition of data. The saturated voltage of the sample after adsorbing the gas slightly increases in each cycle with the time for each vapor.***

Index Terms- ***Sri Lankan Graphite; Gas Sensors; Gas Sensitivity; Doctor Blade Method***

I. INTRODUCTION

A sensor recognizes physical parameters from the environment and converts them into measurable outputs. There are two types of sensors: analog and digital. A gas sensor, meanwhile, is a device that identifies vapors or gases and responds accordingly. The output can be either an analog or digital signal. With this industry's current development, harmful gases are rapidly emitted into the atmosphere and because of this reason identifying toxic gases has become a more important thing nowadays. Therefore, fabricating gas sensors is one of the most essential requirements in the current industry. Moreover, reducing costs and increasing efficiency are major factors in developing these gas sensors.

Among the gases, ammonia (NH_3) is the most harmful gas for both mankind and the environment. Higher concentrations of NH_3 can be found near chemical industries, refrigeration systems, and farms. One of the reasons for kidney disorders and cancers is that NH_3 concentration overdoes in human breath (Han *et al*., 2014). The recommended value of the NH_3 exposure from the US Occupational Safety and Health Administration is 50 ppm over a conventional 8-h workday or a 40-h work week, and a short-term exposure limit of 35 ppm. The National Institute for Occupational Safety and Health recommends the Immediately Dangerous to Life or Health Concentrations are 300 to 500 ppm for 30 to 60 minutes have been reported as a maximum short

exposure tolerance, 5000 to 10000 ppm are reported to be fatal, and exposures for 30 minutes to 2,500 to 6,000 ppm are considered dangerous to life. Therefore, detecting low concentrations of NH_3 is crucial for human health (Travlou *et al*., 2014). Especially in industry, for air quality control, seeking for leakage, and for clinical diagnostics these NH_3 sensors are needed (Han *et al*., 2014). Typically, NH_3 gas sensors are implemented as metal oxide semiconductor gas sensors which operate at high temperatures like 200 to 350 ^{0}C (Bannov *et al*., 2016). Therefore, fabricating a sensor that responds at room temperature is important when considering the above-mentioned recommendation.

Acetone is a colorless, flammable, and volatile organic compound widely used in laboratories, industries, and for cleaning purposes (Zhang *et al*., 2018; Li *et al*., 2023). Because of this wide usage, acetone has had a major impact on human health. According to the Toxicological Profile for Acetone, published in 2022, acetone is a directory that affects neurological, hematological, renal endpoints, respiratory, ocular, and reproductive endpoints. Diabetes is one of the major reasons for causes of cardiovascular diseases and diabetic retinopathy. Recently, around 500 million people have been affected by diabetes, which has had a major impact on our children. , Measuring the acetone concentration in the exhaled breath or skin acetone concentrations can identify diabetics at an early stage. Because a healthy person's acetone concentration in exhaled breath is less than 1 ppm (0.3–0.9 ppm) and a diabetic patient has more than 1.8 ppm (Zhou *et al.*, 2023; Li *et al*., 2022; Liu *et al*., 2013). Therefore, the fabrication of acetone sensors is essential for both industry and society. However, most acetone detection sensors work at high temperatures and have high manufacturing costs (Liu *et al*., 2013). For these reasons, fabricating sensors that work at room temperature and reduce production costs is commercially important.

In day-to-day tasks, ethanol is used for a variety of applications in industry such as food industry, brewing process control and clinical, medical applications. Additionally, ethanol is a highly flammable and toxic and can be explosive when it mixes with air (Pandya *et al*., 2011; Chachuli *et al*., 2023). Also, ethanol can be affected by human health and environment (Chachuli *et al*., 2023). Moreover, headaches, nausea, confusion, dizziness, and balance disorders can happen when humans are inhaled in a high concentration of ethanol vapor (Liao *et al*., 2013). Therefore, identifying ethanol vapor is crucial. Because of these reasons, fabricating an ethanol sensor is both effective and essential for industry and the environment.

Identifying the key aspects of detecting NH_3, acetone, and methanol, this study involved fabricating sensors and analyzing their characteristics for each vapor at room temperature.

II. METERIALS AND METHODS

A. Sample preparation:

A Graphite sample (BCB20) with a 99.1% carbon content was obtained from Bogala Lanka Ltd. in Sri Lanka. The graphite sample was mixed with distilled water and acetone (75wt% acetone) for coating on Fluorine-doped Tin Oxide (FTO) glass plates (Yi *et al*., 2012). A 2cm × 4cm FTO glass plate was divided into two separate parts by removing the conductive FTO layer at the center of the substrate to create the gas sensor. The FTO plates were then cleaned with acetone, washed out using distilled water, and dried. The resistance of the FTO glass plate was measured to ensure that the electric current does not flow through FTO layer from one end to the other end of the substrate. The mixture was then coated onto the FTO using the Doctor Blade method. After that, the sample was heated at 100 ^{0}C for 3 hours in air in an oven to completely evaporate that water, excess air, and acetone. Finally, the sample resistance was measured.

B. Structural and morphological measurements:

The mixture was coated on a non-conductive glass plate for analysis using X-ray Diffraction (XRD) (Rigaku Ultima IV) with CuK_α radiations. The structural properties of the graphite sample were determined by this test. Scanning Electron Microscopy (SEM) analysis was conducted using a Zeiss EVO LS15 SEM machine to observe the surface of the sensor.

© JAN 2026 | IRE Journals | Volume 9 Issue 7 | ISSN: 2456-8880
DOI: https://doi.org/10.64388/IREV9I7-1713855

C. Gas Sensitivity measurements:

The coated sample was placed into a chamber, and gold-coated electrodes were used for the connection. The sensor was connected to the power supply through a resistor, with an input voltage of 5 V applied, as shown in Figure 1. The sensor was then left to stabilize for 1 hour. Once the sensor achieved stable voltage, 1000 ppm vapors were injected into the chamber and the voltage across the resistor was measured over time. After the voltage across the sensor was stabilized, normal air was injected into the gas chamber to remove the gas or vapor inside. During this procedure, the voltage across the resistor was measured over time. This procedure was repeated for each vapor. The gas sensitivity in all the vapors was measured at the room temperature.

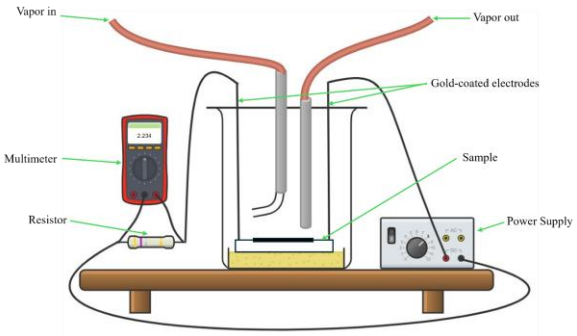

Figure 01: Schematic of the experimental setup used to measure the sensing voltage of the gas sensor

IV. RESULTS AND DISCUSSION

The XRD pattern of the coated graphite sample is shown in Figure 2. This XRD pattern of graphite illustrated a strong diffraction peak at 2θ = 25.970 which corresponds to the (002) plane and other peaks at 2θ = 54.119 and 86.599 which corresponds to the (004) and (006) planes, respectively. The entire peaks match with the peaks of pure graphite, and any additional peaks were not observed by confirming the purity of the used graphite (Popova, 2017; Aladekomot & Bragg, 1990; Li *et al*, 2007; Barnakov *et al*., 2015). X-ray diffraction pattern of our thin films is similar to powder diffraction pattern of XRD by indicating that there is not any preferred orientation of crystallites. It implies that the distribution of crystallites is isotropic. Based on the X-ray diffraction pattern, the following parameters were calculated. The interplane distance d_{00l} for the sample was calculated using Bragg's Law (Popova, 2017).

$$d_{00l} = \lambda/2 \sin\theta_{00l} \rightarrow (1)$$

And Crystallite sizes (D) were calculated using Scherrer equation (Qiu *et al*., 2019).

$$D = \frac{K\lambda}{\beta \cos\theta} \rightarrow (2)$$

Where λ is the radiation wavelength of Cu-Kα radiation (λ =1.54060 Å); θ is the reflection angle for the reflex (00l) (l = 2, 4, or 6); β is the full width at half maximum (FWHM) of XRD peak at angle θ; k is constant specific to the crystal direction (k = 0.9). Calculated values of crystallite sizes are given in table 1.

Table 1: Values of crystallite size found from different XRD peaks

Miller Indices	Diffraction angle (2θ)	Bragg angle (θ)	interplane distance (d) (A^0)	FWHM (deg)	Crystallite size (nm)
(002)	25.97	12.985	3.4281	0.1419	60.00782
(004)	54.12	27.06	1.6932	0.12729	73.19767
(006)	86.64	43.32	1.1227	0.19237	59.28573

© JAN 2026 | IRE Journals | Volume 9 Issue 7 | ISSN: 2456-8880
DOI: https://doi.org/10.64388/IREV9I7-1713855

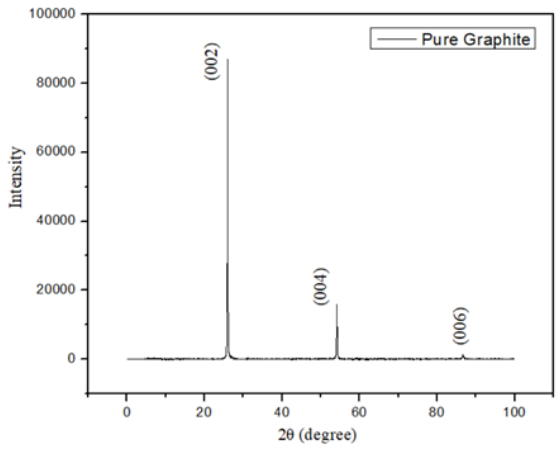

Figure 2: X-ray diffraction (XRD) analysis of Sri Lankan pure graphite.

Figure 3 shows the SEM micrographs of the thin film graphite sample. The particles have an irregular shape similar to any crushed powders. On the top of large particles, few nano-size particles can be observed. The particles are closely packed, and the calculated porosity is 8.98%. This porosity was calculated using the ImageJ software.

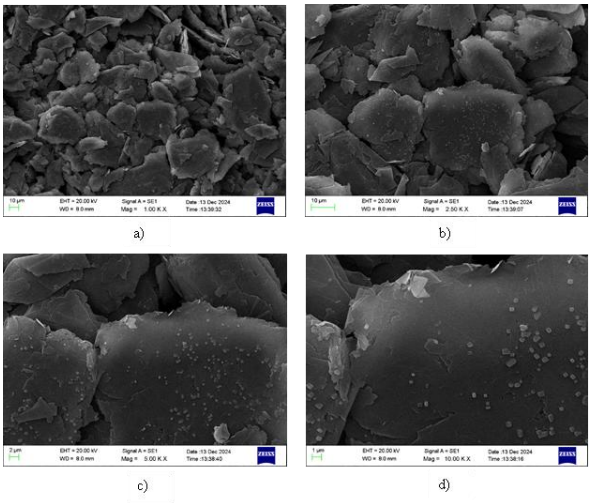

Figure 3: SEM images of the thin film graphite sample at different magnifications: a) 1000x, b) 2500x, c) 5000x, and d) 10000x.

The diameters of the particles were measured using ImageJ software, and a corresponding graph was generated, as shown in Figure 4. The measured diameters ranged from 4 to 70 µm. A manority of particle exhibits the size of 20 µm.

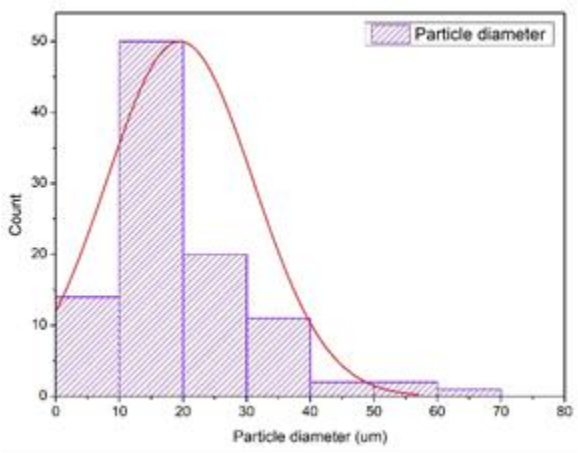

Figure 04: Distribution of particle diameters in the thin film graphite sensor

Figures 5 (a), (b) and (c) show the voltage, current and resistance versus time variation for the NH_3, ethanol and for the actone. According to the graphs, the voltages were increased once sensor absorbed the vapors of NH_3, ethanol and acetone. The resistance of the sensors were increased when it started to absorb. The current through the sample varied inversely with the sensor's resistance. The gas sensitivity was calculated using the following equation.

$$\text{Gas sensitivity} = \frac{|R_g - R_a|}{R_a} \times 100\% \quad \rightarrow \quad (3)$$

where R_a is the sensor resistance in air and Rg is the sensor resistance in target gas (Chakraborthy *et al*., 2022). The resistance and current were calculated using

$$R = \left(\frac{5}{v} - 1\right) s \quad \rightarrow \quad (4)$$

$$I = \left(\frac{5 - v}{R}\right) \quad \rightarrow \quad (5)$$

Where v and s are the voltage measured across the standard resistor and the value of the standard resistor, respectively.

According to the data obtained from the graph, acetone has the highest gas sensitivity at 23.98% compared to NH_3 at 6.37% and ethanol at 7.16%. Addirionally, acetone has the shortest response time and recovery time, at 50 and 22 minutes,

© JAN 2026 | IRE Journals | Volume 9 Issue 7 | ISSN: 2456-8880
DOI: https://doi.org/10.64388/IREV9I7-1713855

respectively. Meanwhile NH_3 has response and recovery times of 110 and 46 minutes, respectively. For ethanol, the respose time was 124 minutes and the recovery time was 22 minutes.

The adsorption of acetone atoms is higher compared to that of ammonia and ethanol atoms. The interaction potential between the gas and the surface of the graphite sample affects the amount of gas adsorbed. The interaction potential depends on Van der Waals forces, chemical bonding, electrostatic interactions and quantum effects.

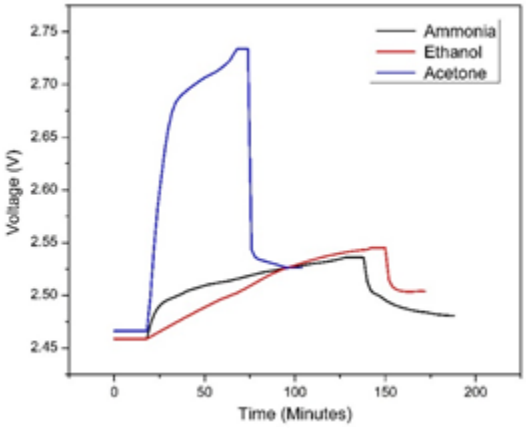

a)

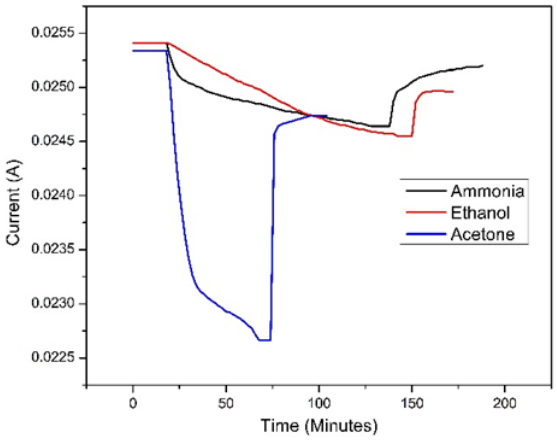

b)

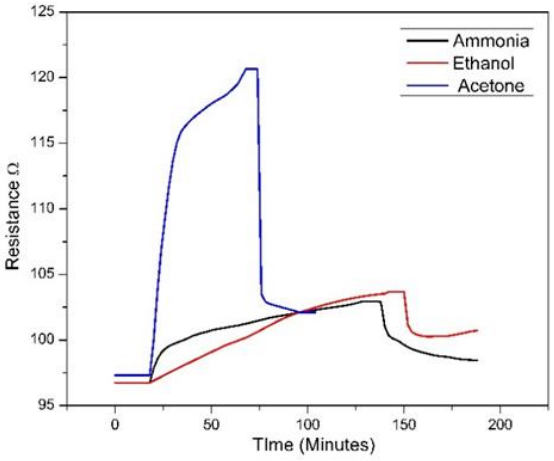

c)

Figure 5: The graphical representations of a) voltage b) current and c) resistance of pure graphite sensor with NH3, ethanol and acetone.

The resistance of the sample increases after adsorbing each vapor due to the oxidation as given below.

$VO + e^- \rightarrow VO^-$

Where V represents the vapor atom. The acceptance of electrons from the conduction band reduces the conductivity of the graphite sample, resulting the increase of the resistivity.

Figure 6 illustrates the three-cycle graph for 1000 ppm NH_3. As depicted, the sensor did not return to its initial value after air was introduced into the chamber. Instead, it stabilized before reaching the starting value. This stabilization may occur because, despite the application of air, the NH_3 adhered to the sensor's surface and did not separate. As a result, the resistance increased and did not return to its initial value. Consequently, with each subsequent cycle, the recovery point was higher than the previous one. Additionally, when comparing response time across the first, second, and third cycles, a decreasing trend is observed. The response time for the first cycle was 110 minutes, reduced to 62 minutes for the second cycle, and further reduced to 60 minutes for the third cycle. This reduction in response time can be attributed to the aforementioned scenario.

© JAN 2026 | IRE Journals | Volume 9 Issue 7 | ISSN: 2456-8880
DOI: https://doi.org/10.64388/IREV9I7-1713855

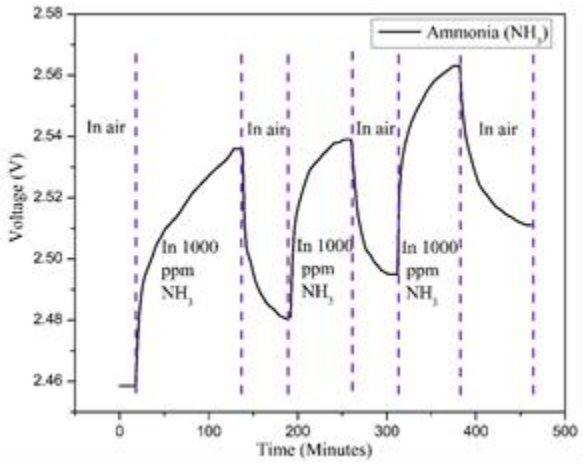

Figure 6: Response of sensor 1000 ppm NH3 gas for three cycles.

Since graphite consists of layers of carbon atoms arranged in a hexagonal lattice, weak van der Waals forces, which are relatively weak compared to chemical bonding, can attract gas molecules to the surface of these layers. This type of adsorption is referred to physisorption, which is reversible and depends on temperature and pressure. Physisorption allows the formation of multiple layers of gas molecules. Physisorption does not involve the formation of chemical bonds, meaning it can occur with various gases. In addition, imperfections, edges, and defects in graphite increase the surface area and provide active sites for gas adsorption. Graphite is composed of stacked graphene layers, with adsorption primarily occurring on the basal planes and edges. While basal planes exhibit weak adsorption, defects and edge sites in graphite can enhance adsorption by providing stronger interaction sites. Some forms of graphite (e.g., activated graphite) may have micropores that increase adsorption capacity due to confinement effects. Introducing defects (e.g., through ion irradiation, oxidation, or plasma treatment) increases adsorption sites and sensitivity. Functionalizing graphite with oxygen-containing groups (e.g., hydroxyl, carboxyl) can enhance gas sensitivity, especially for polar gases like NO_2 or NH_3. Gases such as N_2, O_2, Ar and CO_2 interact via weak Van der Waals forces, leading to low sensitivity unless defects or activation treatments are applied. Gases like NO_2 (electron acceptor) or NH_3 (electron donor) can cause charge transfer, altering the electronic properties of graphite and enhancing sensitivity. In chemiresistive gas sensors, resistance changes due to charge transfer between graphite and adsorbed gases.

Gas adsorption on graphite often follows Langmuir or Brunauer–Emmett–Teller (BET) isotherms, depending on whether monolayer or multilayer adsorption occurs. Lower temperatures and higher pressures favor adsorption, as gas molecules have less kinetic energy to escape the surface. In Langmuir isotherms, it is assumed that each adsorption site can hold only one molecule, meaning no multilayer adsorption occurs, the surface has a fixed number of adsorption sites, all adsorption sites have the same energy, adsorbed molecules do not interact with each other, a dynamic equilibrium exists between adsorption and desorption. In BET isotherms, it is assumed that gas molecules can form multiple layers on the surface, adsorbed molecules in different layers do not interact with each other, adsorption and desorption occur independently for each layer. In BET isotherms, molecules must adsorb onto already adsorbed layers. Therefore, the Langmuir isotherm is faster than BET isotherm. Because our samples take a longer time to response to the vapor and recover, BET isotherms may occur in our samples.

These sites have dangling bonds that can interact with gas molecules more strongly. Some gases, such as oxygen and nitrogen, can insert themselves between graphite layers, forming an intercalation compound. This process can enhance adsorption and may lead to chemical modifications. Furthermore, while bulk graphite has a relatively low surface area, activated graphite (e.g., expanded graphite or graphite oxide) has a much higher porosity, increasing its gas adsorption capacity. Pore structures in activated graphite provide more surface sites for gas molecules to adhere to. In certain cases, gases can form chemical bonds with oxygen-containing functional groups on the graphite surface (e.g., in oxidized graphite or graphene oxide). This chemisorption process is stronger than physisorption and can be used for applications like gas sensing and storage. Though graphite mainly undergoes physisorption, some gases (like oxygen, hydrogen, and fluorine) can chemisorb at defect sites or under specific conditions (e.g., plasma activation), leading

to stronger, irreversible bonding. Higher surface area, doping and defect density lead to greater adsorption and better sensing performance. At lower temperatures, physisorption dominates, leading to reversible gas adsorption. At higher temperatures, desorption occurs more readily, reducing sensitivity unless chemisorption takes place (e.g., O_2 at defect sites).

Graphite can adsorb ammonia (NH_3), ethanol (C_2H_5OH) and acetone (C_3H_6O) vapors mainly through physisorption. Ammonia molecules are held on the graphite surface by weak van der Waals forces. Since physisorption is weak, ammonia, ethanol and acetone vapors can be easily desorbed by lowering the pressure or increasing the temperature. Lower temperatures favor ammonia, ethanol and acetone adsorption (exothermic process). Therefore all our samples were measured at the room temperature. The carbonyl group (C=O) in acetone can interact with the delocalized π-electrons of graphite. The hydroxyl (-OH) group in ethanol interacts weakly with the delocalized π-electron cloud of graphite.

We have studied the gas sensing properties of biomass based carbon particles (Ranasinghe *et al*., 2024; Samarahewa *et al*., 2024). Those carbon films behaved in a similar fashion after adsorbing gases and vapors. Although the graphene and graphite oxide based gas sensors have been widely found, only a few gas sensing research work of pure graphite based gas sensors can be found. Graphite gas sensors have been employed to detect volatile organic compounds (VOCs) such as ethylene (Manzoli *et al*., 2011). Graphite mixed with metal oxides has been used to sense 2-chloroethyl ethyl sulfide (2-CEES) (Yang *et al*., 2024). Pure graphite has not been previously employed to detect ammonia, acetone and ethanol vapors.

V. CONCLUSION

In this study, Sri Lankan natural graphite was utilized for sensor preparation. Acetone and distilled water were employed in the fabrication process, and the doctor blade method was used to coat the graphite mixture onto the FOT glass. According to XRD patterns, the phase of pure graphite could be crystallized in thin film form, and determined the average crystallite size to be 64.16374 nm. Gas sensitivity measurements were conducted at 1000 ppm for NH_3, ethanol, and acetone vapors at room temperature. Among these, acetone demonstrated the highest sensitivity. Additionally, acetone exhibited the shortest response and recovery times. The porous structure and higher effective surface area of our graphite films are responsible for the higher gas sensitivity of our samples. The weak van der Waals force between vapor molecules and graphite surface is the main cause of adsorption. Because the adsorption of ethanol and acetone vapors is higher at lower temperatures in exothermic process, the gas sensitivity of all the samples was measured at the room temperature. In addition, physisorption leads at lower temperatures, guiding to reversible gas adsorption. The interaction of carbonyl group or hydroxyl of the vapor with graphite is the origin of the gas sensitivity of these vapors. Future work will involve testing these samples at different temperatures and doping with various materials to further enhance the gas sensitivity and reduce the response and recovery times.

ACKNOWLEDGMENT

The authors gratefully acknowledge the Bogala Graphite Lanka PLC for providing the graphite samples used in this research. We extend our sincere to Mr. Anura Liyanage and Mr. Saliya Gamlath for their invaluable assistance in this matter.

REFERENCES

[1] Aladekomo, J. B., and Bragg, R. H. (1990). STRUCTURAL TRANSFORMATIONS INDUCED IN GRAPHITE BY GRINDING: ANALYSIS OF 002 X-RAY DIFFRACTION LINE PROFILES. *Carbon* 28(6): 897-906.

[2] Bannov, A. G., Prášek, J., Jašek, O., Shibaev, A. A., and Zajíčková, L. (2016). Investigation of Ammonia Gas Sensing Properties of Graphite Oxide. *Procedia Engineering* 168: 231–234. https://doi.org/10.1016/j.proeng.2016.11.169

[3] Barnakov, C. N., Khokhlova, G. P., Popova, A. N., Sozinov, S. A., and Ismagilov, Z. R. (2015).

XRD characterization of the structure of graphites and carbon materials obtained by the low-temperature graphitization of coal tar pitch. *Eurasian Chemico-Technological Journal* 17(2): 87–93. https://doi.org/10.18321/ectj198

[4] Chachuli, S. A. M., Noor, M. L. H., Coban, O., Shamsudin, N. H., and Idris, M. I. (2023). Characteristic of graphene-based thick film gas sensor for ethanol and acetone vapor detection at room temperature. *Indonesian Journal of Electrical Engineering and Computer Science* 32(3): 1384–1391. https://doi.org/10.11591/IJEECS.V32.I3.PP1384-1391

[5] Chakraborthy, A., Nuthalapati, S., Nag, A., Afsarimanesh, N., Alahi, M. E. E., and Altinsoy, M. E. (2022). A Critical Review of the Use of Graphene-Based Gas Sensors. *Chemosensors* 10(9): 355. https://doi.org/10.3390/chemosensors10090355

[6] Han, J. W., Kim, B., Li, J., and Meyyappan, M. (2014). A carbon nanotube based ammonia sensor on cellulose paper. *RSC Advances* 4(2): 549–553. https://doi.org/10.1039/c3ra46347h

[7] Li, Z. Q., Lu, C. J., Xia, Z. P., Zhou, Y., and Luo, Z. (2007). X-ray diffraction patterns of graphite and turbostratic carbon. *Carbon* 45(8): 1686–1695. https://doi.org/10.1016/j.carbon.2007.03.038

[8] Li, C., Choi, P. G., Kim, K., and Masuda, Y. (2022). High performance acetone gas sensor based on ultrathin porous NiO nanosheet. *Sensors and Actuators B: Chemical* 367. 132143.https://doi.org/10.1016/J.SNB.2022.132143

[9] Li, C., Kim, K., Fuchigami, T., Asaka, T., Kakimoto, K., and Masuda, Y. (2023). Acetone gas sensor based on Nb_2O_5 @SnO_2 hybrid structure with high selectivity and ppt-level sensitivity. *Sensors and Actuators B: Chemical* 393: 134144. https://doi.org/10.1016/J.SNB.2023.134144

[10] Liao, W. Z., Dai, C. L., and Yang, M. Z. (2013). Micro ethanol sensors with a heater fabricated using the commercial 0.18 μm CMOS process. *Sensors* 13(10): 12760–12770. https://doi.org/10.3390/s131012760

[11] Liu, F., Chu, X., Dong, Y., Zhang, W., Sun, W., and Shen, L. (2013). Acetone gas sensors based on graphene-$ZnFe_2O_4$ composite prepared by solvothermal method. *Sensors and Actuators B: Chemical* 188: 469–474. https://doi.org/10.1016/J.SNB.2013.06.065

[12] Manzoli, A., Steffens, C., Paschoalin, R.T., Correa, A.A., Alves, W.F., Leite, F.L., Herrmann, P.S.P. (2011). Low-Cost Gas Sensors Produced by the Graphite Line-Patterning Technique Applied to Monitoring Banana Ripeness. *Sensors* 11(6): 6425-6434. doi: 10.3390/s110606425

[13] Pandya H.J., Chandra S., and Vyas A.L. (2011). Fabrication and Characterization of Ethanol Sensor Based on RF Sputtered ITO Films. *Sensors & Transducers Journal* 10:141–150.

[14] Popova, A. N. (2017). Crystallographic analysis of graphite by X-Ray diffraction. *Coke and Chemistry* 60(9): 361–365. https://doi.org/10.3103/S1068364X17090058

[15] Qiu, T., Yang, J., Bai, X., and Wang, Y. (2019). The preparation of synthetic graphite materials with hierarchical pores from lignite by one-step impregnation and their characterization as dye absorbents. *RSC Advances* 9(22): 12737–12746. https://doi.org/10.1039/c9ra00343f

[16] Ranasinghe, R.A.S.R., Rathnathilaka, K.A.C., Karunarathna, P.G.D.C.K. and Samarasekara, P. (2024). Carbon gas sensors synthesized using acacia auriculiformis tree branches to detect methanol, ethanol, acetone vapors and ammonia gas. *Ceylon Journal of Science* 53(2): 207-218. https://doi.org/10.4038/cjs.v53i2.8412

[17] Samarahewa, C.A., Dehipawala, S. and Samarasekara P. (2024). Optimization of gas sensitivity of CuO/carbon composites with carbon particles synthesized from acacia auriculiformis branches. *STM Journals: International Journal of Membranes* 1(1): 22-30.

[18] Travlou, N. A., Seredych, M., Rodriguez-Castellon, E., and Bandosz, T. J. (2014). Activated carbon-based gas sensors: Effects of surface features on sensing mechanism. *Journal of Materials Chemistry A* 3: 3821-3831.

https://doi.org/https://doi.org/10.1039/C4TA06161F

[19] Yang, L.P., Cheng, W., Yan, W., Wen, L., Xia, C., Sun, C., Hu D., Zhao, Y., Guo, X., Zeng W. and Wang S. (2024). Highly Sensitive and Selective MEMS Gas Sensor Based on WO_3/Al_2O_3/Graphite for 2-Chloroethyl Ethyl Sulfide (2-CEES) Detection. *Chemosensors* 12(1):5 https://doi.org/10.3390/chemosensors12010005

[20] Yi, M., Shen, Z., Zhang, X., and Ma, S. (2012). Achieving concentrated graphene dispersions in water/acetone mixtures by the strategy of tailoring Hansen solubility parameters. *Journal of Physics D: Applied Physics* 46: 025301 https://doi.org/10.1088/0022-3727/46/2/025301

[21] Zhang, R., Wang, Y., Zhang, Z., and Cao, J. (2018). Highly sensitive acetone gas sensor based on g-C_3N_4 decorated $MgFe_2O_4$ porous microspheres composites. *Sensors* 18(7): 2211. https://doi.org/10.3390/s18072211

[22] Zhou, H., Ramaraj, S. G., Ma, K., Sarker, M. S., Liao, Z., Tang, S., Yamahara, H., and Tabata, H. (2023). Real-time detection of acetone gas molecules at ppt levels in an air atmosphere using a partially suspended graphene surface acoustic wave skin gas sensor. *Nanoscale Advances* 5(24): 6999–7008. https://doi.org/10.1039/d3na00914a